Check for updates

Patient-specific computational flow simulation reveals significant differences in paravisceral aortic hemodynamics between fenestrated and branched endovascular aneurysm repair

Kenneth Tran, MD,[a] Celine Deslarzes-Dubuis, MD,[b] Sebastien DeGlise, MD,[b] Adrien Kaladji, MD,[c] Weiguang Yang, PhD,[d] Alison L. Marsden, PhD,[d] and Jason T. Lee, MD,[a] *Stanford, CA; Lausanne, Switzerland; and Paris, France*

ABSTRACT

Background: Endovascular aneurysm repair with four-vessel fenestrated endovascular aneurysm repair (fEVAR) or branched endovascular aneurysm repair (bEVAR) currently represent the forefront of minimally invasive complex aortic aneurysm repair. This study sought to use patient-specific computational flow simulation (CFS) to assess differences in postoperative hemodynamic effects associated with fEVAR vs bEVAR.

Methods: Patients from two institutions who underwent four-vessel fEVAR with the Cook Zenith Fenestrated platform and bEVAR with the Jotec E-xtra Design platform were retrospectively selected. Patients in both cohorts were treated for paravisceral and extent II, II, and V thoracoabdominal aortic aneurysms. Three-dimensional finite element volume meshes were created from preoperative and postoperative computed tomography scans. Boundary conditions were adjusted for body surface area, heart rate, and blood pressure. Pulsatile flow simulations were performed with equivalent boundary conditions between preoperative and postoperative states. Postoperative changes in hemodynamic parameters were compared between the fEVAR and bEVAR groups.

Results: Patient-specific CFS was performed on 20 patients (10 bEVAR, 10 fEVAR) with a total of 80 target vessels (40 renal, 20 celiac, 20 superior mesenteric artery stents). bEVAR was associated with a decrease in renal artery peak flow rate (-5.2% vs $+2.0\%$; $P < .0001$) and peak pressure (-3.4 vs $+0.1\%$; $P < .0001$) compared with fEVAR. Almost all renal arteries treated with bEVAR had a reduction in renal artery perfusion ($n = 19$ [95%]), compared with 35% ($n = 7$) treated with fEVAR. There were no significant differences in celiac or superior mesenteric artery perfusion metrics ($P = .10$-.27) between groups. Time-averaged wall shear stress in the paravisceral aorta and branches also varied significantly depending on endograft configuration, with bEVAR associated with large postoperative increases in renal artery ($+47.5$ vs $+13.5\%$; $P = .002$) and aortic time-averaged wall shear stress ($+200.1\%$ vs -31.3%; $P = .001$) compared with fEVAR. Streamline analysis revealed areas of hemodynamic abnormalities associated with branched renal grafts which adopt a U-shaped geometry, which may explain the observed differences in postoperative changes in renal perfusion between bEVAR and fEVAR.

Conclusions: bEVAR may be associated with subtle decreases in renal perfusion and a large increase in aortic wall shear stress compared with fEVAR. CFS is a novel tool for quantifying and visualizing the unique patient-specific hemodynamic effect of different complex EVAR strategies.

Clinical Relevance: This study used patient-specific CFS to compare postoperative hemodynamic effects of four-vessel fenestrated endovascular aneurysm repair (fEVAR) and branched endovascular aneurysm repair (bEVAR) in patients with complex aortic aneurysms. The findings indicate that bEVAR may result in subtle reductions in renal artery perfusion and a significant increase in aortic wall shear stress compared with fEVAR. These differences are clinically relevant, providing insights for clinicians choosing between these approaches. Understanding the patient-specific hemodynamic effects of complex EVAR strategies, as revealed by CFS, can aid in future personalized treatment decisions, and potentially reduce postoperative complications in aortic aneurysm repair. (JVS—Vascular Science 2024;5:100183.)

Keywords: Computational flow dynamics; Simulation; Fenestrated EVAR; Branched EVAR

Endovascular repair of thoracoabdominal aortic aneurysms with custom-made devices (CMDs) currently represents the forefront of minimally invasive complex aortic aneurysm treatment.[1,2] CMD endograft designs consist of two distinct strategies for providing renovisceral branch perfusion—fenestrated endovascular aneurysm repair (fEVAR) and branched endovascular aneurysm repair (bEVAR).[1,3] fEVAR devices are comprise of prefabricated, reinforced fenestrations that allow for the placement of stent grafts into the origins of target branch arteries. In contrast, bEVAR endografts are built with antegrade or retrograde portals that allow for bridging stent grafts to be placed into target arteries. Each strategy results in unique differences in flow lumen morphology for blood delivery to target branch vessels. Both fEVAR and bEVAR have gained popularity in the United States and Europe, with commercially available systems demonstrating favorable early- and mid-term outcomes for treating complex aortic pathology at select centers.[4-6] However, despite increasing adoption of CMDs over the last decade, concerns remain regarding the durability of branch grafts. The latest reports indicate up to a 20% risk of early and late branch-related adverse events, including branch graft occlusion, which is associated with significant morbidity.[6-10] In addition, the optimal design configuration of fenestrated and branched grafts is poorly understood and is currently solely based on anatomical constraints, without consideration of how altered flow geometry from branch placement or type (eg, flare angle, antegrade, retrograde, internal or external portals) can adversely affect branch-vessel hemodynamics and thus increase thrombotic risk.[11,12]

Recently, computational fluid dynamic (CFD) modelling methods have been applied to study hemodynamic changes associated with various endograft designs. However, owing to the complexity of multibranch aortic model generation and flow simulation, studies using CFD modeling techniques in complex EVAR seldomly evaluate more than one or two patient geometries.[13-18] Existing CFD studies involving thoracoabdominal aortic aneurysm complex EVAR remain limited to idealized, nonpatient-specific graft geometries.[15,17] To date, no studies have compared CFD-derived hemodynamic changes after implantation of fEVAR and bEVAR devices in a cohort of real-world patients.

In this retrospective study, we aimed to use patient-specific computational flow simulation (CFS) to investigate the hemodynamic differences between patients undergoing four-vessel fEVAR and bEVAR. We hypothesized that fEVAR device implantation results in flow geometry which more closely mimics native vessel anatomy, and thus may be associated with less significant changes in branch vessel hemodynamics compared with bEVAR. Identifying potential hemodynamic differences between graft geometries may have important

ARTICLE HIGHLIGHTS

- **Type of Research:** Human in vitro study
- **Key Findings:** Twenty patients with thoracoabdominal aortic aneurysms were analyzed using patient-specific computational flow simulation (CFS) techniques. Adverse renal perfusion and wall shear stress metrics were noted to more frequently occur after repair with branched endografts compared to fenestrated endografts.
- **Take Home Message:** CFS techniques may be useful for future clinical studies to optimizing patient hemodynamics during complex endovascular aneurysm repair.

implications regarding long-term branch vessel stability.[9,10,19]

METHODS

Study design. This study was a multi-institutional collaboration between Lausanne University Hospital (Lausanne, Switzerland), Rennes University Hospital (Rennes, France) and Stanford University (California). Patient and radiologic data were obtained from a prospectively maintained databases of patients undergoing complex EVAR. Patients undergoing fEVAR and bEVAR was sourced from Rennes University Hospital and Lausanne University Hospital, respectively. Data was then used for subsequent CFS analysis by a multidisciplinary team with experience in CFS (Stanford University). This study protocol was approved by each institution's respective ethics committee. Owing to the retrospective nature of the study, advanced signed informed consent was not obtained.

Patient cohort. We selected a total of 20 representative patients with paravisceral and thoracoabdominal aortic aneurysms who underwent fEVAR with four fenestrated renovisceral branches (n = 10) and bEVAR with four directional branches (n = 10). fEVAR and bEVAR patients were treated with the Cook Zenith Fenestrated platform (Cook Medical, Bloomington, IN) and the Jotec E-xtra Design Engineering custom-made endograft (JOTEC GmbH, Hechingen, Germany). All patients were treated within the device instructions-for-use and had high-resolution preoperative and postoperative computed tomography angiography imaging available for review. For the purposes of this comparative study, we only included patients without postoperative graft-related complications (eg proximal endoleak, branch stenosis, or occlusion). Four patients in each cohort required proximal thoracic extension to obtain the proximal seal, either in a staged or concurrent intervention. In addition, main body graft diameters were matched between cohorts to decrease diameter-dependent differences in hemodynamics. Branch components in both groups

consisted of primarily Bentley BeGrafts (Bentley Innomed GmbH, Hechingen, Germany). For bEVAR, a combination of antegrade, retrograde, internal and external branch portals were used. A range of main body graft diameters (30-42 mm) was purposefully selected.

Patient-specific geometry and in-flow conditions. Preoperative and early postoperative computed tomography angiography scans were used to extract native aneurysm and postoperative stent geometry (Fig 1, A and B). Individual patient hemodynamic parameters, including average outpatient systolic and diastolic blood pressures, heart rate, and body habitus (height and weight), were collected. Body surface area was then estimated using the patient's height and weight, and in turn used to generate an allometrically scaled supraceliac inflow waveform according to the equation $aortic\ flow\ \left(\frac{mL}{s}\right) = 16.4(body\ surface\ area)^{1.56}$. This scaled waveform has been has previously been validated using phase contrast magnetic resonance imaging to accurately estimate patient-specific in-flow hemodynamics in patients with abdominal aortic aneurysms.[20]

Three-dimensional modelling and mesh generation. Methods for extraction of aortic geometry into a finite element model has been previously described.[21] Briefly, using an open source CFD modeling pipeline (SimVascular; Open Source Medical Software Corp, San Diego, CA), aortic and renovisceral branch geometry was segmented from zone 3 of the aorta to the aortic bifurcation using two dimensional contours. Contours were spaced every 2 to 3 mm near the branch vessel origins with wider 10- to 20-mm spacing at the proximal and distal aorta. These contours are then lofted into three-dimensional models and converted into a finite element volume mesh. A variable mesh size was used to optimize computation time and hemodynamic parameter estimation based upon prior mesh convergence studies.[21] A minimum mesh size of 0.3 mm was used for the branches, 0.5 mm for the paravisceral aorta, and 1 mm for areas outside the region of interest (Fig 1, C). Care was taken to accurately model branch vessel origins (Fig 2, A and B).

Vessel outlet boundary conditions. Branch vessel and distal aortic outlets were modeled as a three-element lumped parameter models (eg Windkessel models), which consists of three parameters: a proximal resistor, capacitor, and distal resistor.[22] These parameters represent the resistance of the outlet artery, compliance of the outlet vessel, and resistance of the downstream vascular bed, respectively. Proximal resistor, capacitor, and distal resistor parameters were tuned individually to match patient systolic and diastolic blood pressure values. We used physiological flow splits from the literature with 25% of total inlet flow to the celiac artery, 31% to the superior mesenteric artery (SMA), and 22% to each renal

artery.[23] For high-resistance vascular beds (eg, resting mesenteric and distal aortic outlets) and low-resistance vascular beds (ie, renal arteries), 94.4% and 72.0% of total resistance was assigned to the distal resistor parameter, respectively.[16] Inflow and outlet conditions were kept equivalent between preoperative and postoperative simulations for each patient.

Flow simulation. Preoperative and postoperative pulsatile flow simulations were performed using SimVascular software with a noncompressible Navier-Stokes flow solver. Blood viscosity was assumed to be non-Newtonian with a viscosity of 0.04 P with a density of 1.06 g/cm^3. Walls were defined as rigid with a no-slip velocity condition. A total of five cardiac cycles were simulated with a time-step size of 1/500th of a cardiac cycle. Minimum residuals required was 1×10^{-4}. Results from the last cardiac cycle were saved with a sampling frequency of 50 per cardiac cycle. Simulations were performed on a 72-core high-performance computational cluster with an average computation time between 48 and 72 hours.

Parameter analysis and statistics. Hemodynamic parameters including pressure waveforms, flow rates and time-averaged wall shear stress (TAWSS) at the aorta and branches were calculated. TAWSS is a measure of local near-wall stresses, which plays a critical role in endothelial and red blood cell and platelet functions. Abnormally low or high TAWSS values are associated with thrombus deposition and atherogenesis.[24] TAWSS was specifically evaluated in the paravisceral aorta, defined as the region from 1.0 cm above the celiac origin to 1.0 cm below the lowest renal artery origin. Values were compared between preoperative and postoperative models using Wilcoxon signed-rank tests, and between fEVAR/bEVAR groups using Wilcoxon rank-sum tests. A systematic parameter analysis was also conducted on a representative patient from each cohort by varying inlet flow rate, arterial pressure (resistance), and pulse pressure (compliance) to assess the effect of variations in boundary conditions on estimated hemodynamics. Each variable was varied independently with a value of one standard deviation above and below the mean. A P value of $<.05$ was considered statistically significant for all analyses. All calculations were performed in Stata SE16.0 (StataCorp LP, College Station, TX). Paraview Visualization ToolKit (Los Alamos National Laboratory, Sante Fe, NM) was used for visualization of TAWSS and flow streamlines.

RESULTS

Preoperative and postoperative patient-specific flow simulations were performed on 10 patients undergoing fEVAR and 10 patients undergoing bEVAR. Demographic, anatomical, and device-related variables for the two cohorts are listed in Table I. There were no significant differences in overall demographics and
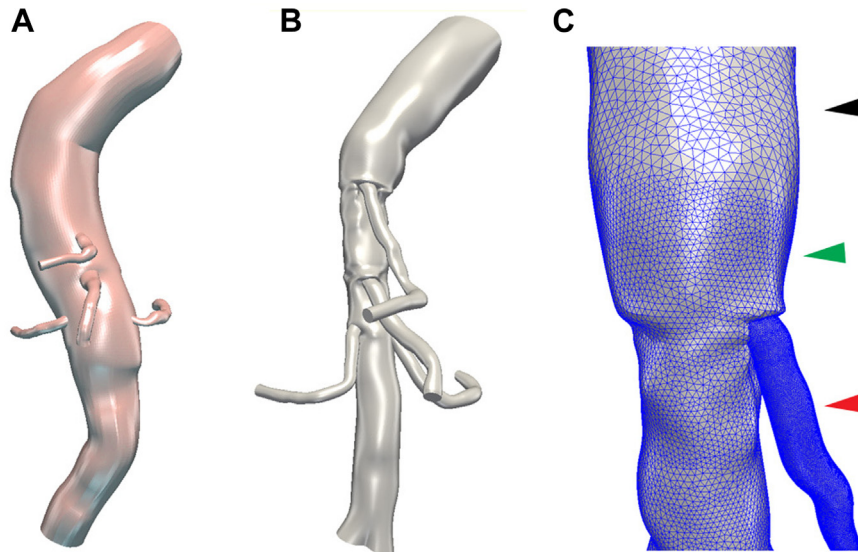
Fig 1. (A) Preoperative thoracoabdominal aortic aneurysm model. **(B)** Postoperative aortic model after four-vessel branched endovascular aneurysm repair. **(C)** Variable-size finite-element mesh model depicting 1.0 mm (*black arrow*), 0.5 mm (*green arrow*), and 0.3 mm (*red arrow*) mesh elements.
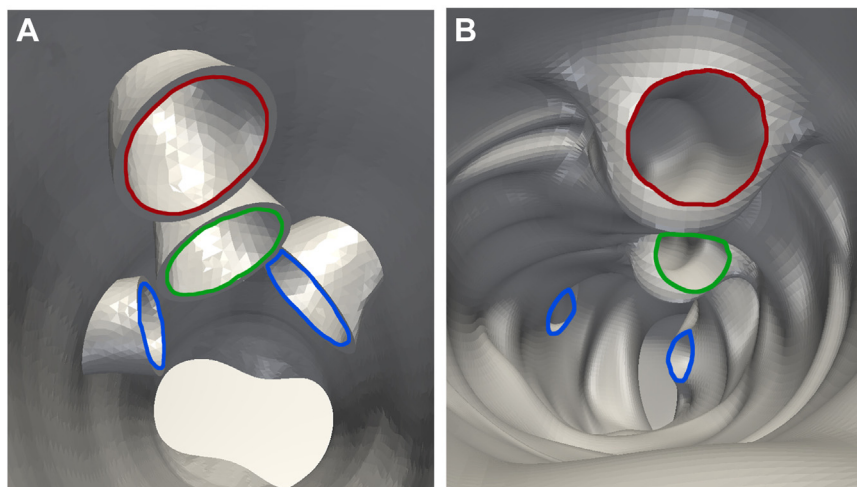

Fig 2. Intraluminal perspective of renovisceral branch ostia in a patient with **(A)** four-vessel fenestrated grafts and **(B)** four-vessel branched grafts in the celiac, superior mesenteric and bilateral renal arteries. Outlines: *red*, celiac artery; *green*, superior mesenteric artery (SMA); *blue*, renal arteries.

comorbidities, with similar prevalences of coronary artery disease, heart failure, diabetes, and kidney disease. Patients in the fEVAR cohort were more commonly treated for paravisceral and extent IV thoracoabdominal aneurysms (n = 8 [80%]), whereas bEVAR patients were more commonly treated for extent II, III, IV, or V thoracoabdominal aortic aneurysms (n = 7 [70%]). The median aneurysm diameter was similar between cohorts (56 mm vs 61.5 mm; *P* = .14). Main body device diameters were similar between cohorts and ranged between 30 and 42 mm. All patients in the fEVAR cohort received a celiac, superior mesenteric, and bilateral renal artery

fenestrated branch stents, with no significant differences in preoperative peak branch pressure or flow rates (*P* = .16-.84) (Supplementary Table I). Allometrically scaled inflow waveform values were also noted to be similar between groups (*P* = .81) (Supplementary Fig 1). In the bEVAR cohort, directional branches were used for all visceral target arteries with a total of 40 branch portals (19 internal and 21 external). Internal branch geometry was more frequently used for the celiac (n = 8 [80%]) and SMA (n = 5 [50%]), whereas renal arteries were more often configured with external branch portals (n = 12 [60%]). A single retrograde internal branch was

Table I. Demographics and anatomical and device-related variables stratified by fenestrated endovascular aneurysm repair (*fEVAR*) and branched endovascular aneurysm repair (*bEVAR*) groups

Variables	fEVAR	bEVAR	*P* value
Patient demographics			
Age, years	83 [70-90]	82 [62-87]	.59
Male gender	6 (60)	8 (80)	.63
Coronary artery disease	5 (50)	4 (40)	.99
Congestive heart failure	1 (10)	0 (0)	.99
Hypertension	6 (60)	10 (100)	.09
Diabetes	3 (30)	1 (10)	.58
Chronic kidney disease	2 (20)	0 (0)	.47
Aneurysm and device factors			
Aneurysm extent			
Paravisceral	3 (30)	0 (0)	-
Extent IV	5 (50)	3 (30)	
Extent III	0 (0)	3 (30)	
Extent V	2 (10)	1 (10)	
Extent II	0 (0)	3 (30)	
Aneurysm diameter, mm	56 [50-70.5]	61.5 [52-80]	.14
Endograft diameter, mm	34 [30-40]	37 [30-42]	.94
Celiac stent	10 (100)	10 (100)	-
SMA stent	10 (100)	10 (100)	-
Renal stent	20 (100)	20 (100)	-

SMA, Superior mesenteric artery.
P value based on Fisher exact test or Wilcoxon rank sum test for categorical and continuous variables, respectively.
Values are median [interquartile range] or number (%).

used for a right renal artery with a cranial target artery orientation.

Branch perfusion. Postoperative changes (Δ) in peak branch pressure and flow rate stratified by cohort are displayed in Fig 3. In the celiac artery, there were no significant differences between fEVAR vs bEVAR cohorts in either peak pressure Δ (median, −1.32 mm Hg [interquartile range (IQR), −4.82 to 3.03 mm Hg] vs +0.31 mm Hg [IQR, −0.08 to 5.36 mm Hg]; *P* = .22; for fEVAR vs bEVAR, respectively) or peak flow rate Δ (median, −1.7 mL/s [IQR, −4.25 to 2.41 mL/s] vs 0.27 mL/s [IQR, −0.92 to 5.08 mL/s]; *P* = .19). Similarly, endograft type was not associated with differences in peak pressure Δ (median, −1.89 mm Hg [IQR, −2.22 to −0.35 mm Hg] vs −1.19 mm Hg [IQR, −2.65 to 0.56 mm Hg]; *P* = .36) or peak flow rate Δ (median, −2.4 mL/s [IQR, −4.01 to −0.96 mL/s] vs 0.28 mL/s [IQR, −0.13 to 0.43 mL/s]; *P* = .36) in the SMA. However, bEVAR was associated with a small but statistically significant decrease in both renal artery peak pressure Δ (median, 1.04 mm Hg [IQR, −0.67 to 1.85 mm Hg] vs −3.07 mm Hg [IQR, −5.58 to −1.08 mm Hg]; *P* < .0001) and peak flow rate Δ (median, 0.28 mL/s [IQR, −0.14 to 0.43 mL/s] vs −0.58 mL/s [IQR, −1.09 to −0.28 mL/s]; *P* = .19). Overall, the relative decrease in perfusion

was small with a decrease in the renal artery peak flow rate (−5.2% vs +2.0%; *P* < .0001) and peak pressure (−3.4% vs +0.1%; *P* < .0001) compared with fEVAR. Almost all renal arteries treated with bEVAR had a reduction in renal artery perfusion (n = 19 [95%]), compared with 35% (n = 7) treated with fEVAR. Most patients experienced a <10% relative reduction in renal peak flow (Fig 4). Of patients with a >10% decrease in flow rate (n = 4), the majority of renal stents (n = 3) adopted a U-shaped geometry associated with abnormal hemodynamics on streamline analysis (Fig 5). A representative bEVAR patient with postoperative decrease in renal perfusion is demonstrated in Fig 6. There was no association between external and internal branch portal configuration and changes to renal peak pressure (*P* = .99) or flow (*P* = .85).

Branch wall shear stress. There were significant differences in postoperative changes in branch vessel TAWSS between the fEVAR and bEVAR groups. Compared with fEVAR, bEVAR was associated with a greater postoperative increase in TAWSS in the renal arteries (median, 0.9 dynes/cm^2 [IQR, −3.5 to 10.4 dynes/cm^2] vs +10.5 dynes/cm^2 [IQR, 6.2 to 14.2 dynes/cm^2]; *P* = .006). The median renal artery TAWSS in the bEVAR cohort was associated with an increase of 6.0 dynes/cm^2
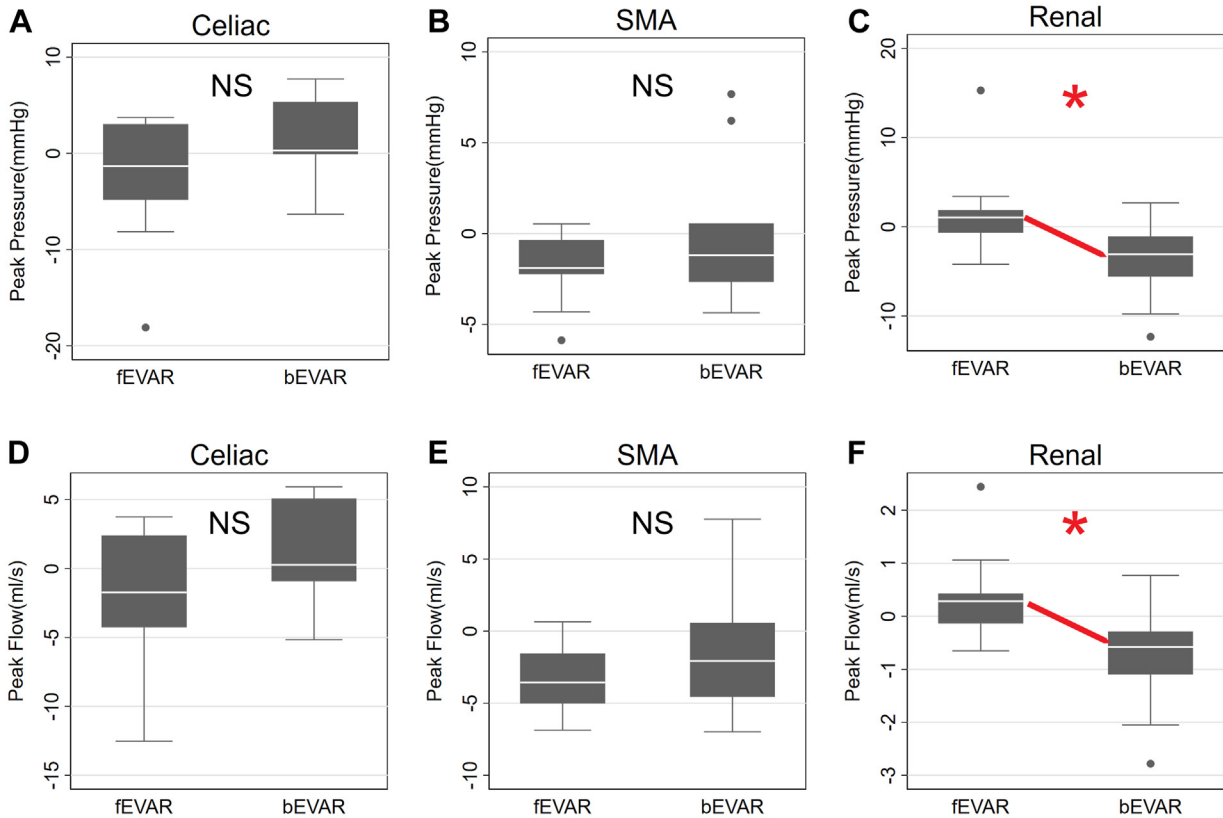
Fig 3. Relative postoperative changes (Δ) in branch hemodynamics stratified by fenestrated endovascular aneurysm repair (*fEVAR*) and branched endovascular aneurysm repair (*bEVAR*) patients. **(A)** Δ peak pressure in the celiac artery. **(B)** Δ peak pressure in the superior mesenteric artery. **(C)** Δ peak pressure in the renal arteries. **(D)** Δ peak flow rate in the celiac artery **(E)** Δ peak flow rate in the superior mesenteric artery. **(F)** Δ peak flow rate in the renal arteries.
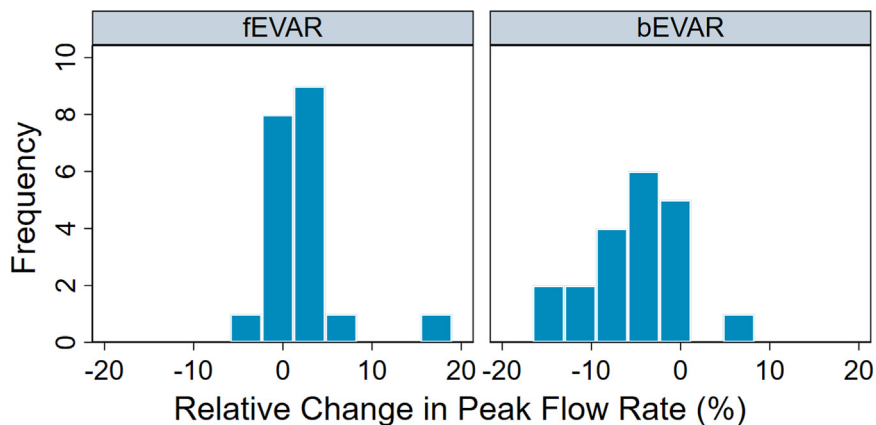

Fig 4. Histogram frequency distribution of relative changes in renal artery peak flow rate following fenestrated endovascular aneurysm repair (*fEVAR*) and branched endovascular aneurysm repair (*bEVAR*). bEVAR was consistently associated with a small decline in renal artery perfusion postoperatively.

postoperatively (median, 26.3 dynes/cm^2 [IQR, 18.8-28.6 dynes/cm^2] vs 33.3 dynes/cm^2 [IQR, 26.5-43.6 dynes/cm^2]; $P = .0003$; preoperative vs postoperative, respectively; paired t test). This corresponded with a relative median increase of +47.5%. After fEVAR, no significant

paired postoperative changes in renal TAWSS were found (median, 32.2 dynes/cm^2 [IQR, 28.1-39.2 dynes/cm^2] vs 36.1 dynes/cm^2 [IQR, 28.5-41.7 dynes/cm^2]; $P = .39$). In the SMA, fEVAR was associated with a greater postoperative increase in TAWSS (median, 8.6 dynes/cm^2
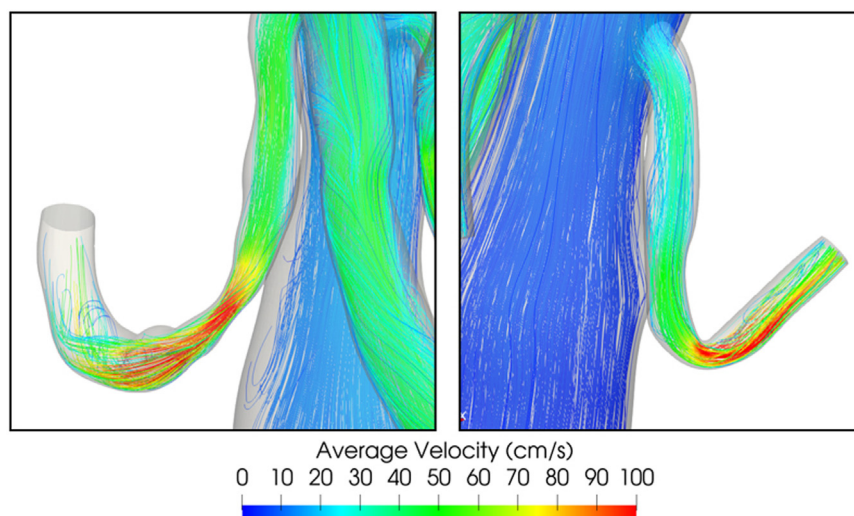
Fig 5. Representative three-dimensional streamline analysis on patients treated with branched endovascular aneurysm repair (bEVAR) with renal branch stents adopting a U-shaped geometry. Abnormal flow hemodynamics demonstrated in red regions.

[IQR, 4.2-11.4 dynes/cm^2] vs 2.9 dynes/cm^2 [IQR, −1.4 to 5.1 dynes/cm^2]; P = .023) compared with bEVAR. The median SMA TAWSS in the fEVAR cohort was found to increase by 7.9 dynes/cm^2 after device implantation (median, 21.9 dynes/cm^2 [IQR, 19.3-24.1 dynes/cm^2] vs 29.8 dynes/cm^2 [IQR, 26.4-32.7 dynes/cm^2]; P = .0069), whereas no significant change was found after bEVAR (median, 20.7 dynes/cm^2 [IQR, 13.8-25.1 dynes/cm^2] vs 22.7 dynes/cm^2 [IQR, 19.6-25.5 dynes/cm^2]; P = .13). No significant differences in celiac TAWSS were found between EVAR groups (P = .13).

Aortic hemodynamics. Aortic inlet (median, 1.8 [IQR, 1.27-6.9] vs 2.1[IQR, 0.1-3.6]; P = .28) and outlet pressures (median, 1.4 [IQR, 1.23-4.7] vs 1.73[IQR, −0.1 to 3.2]; P = .22) were minimally increased after both fEVAR and bEVAR with no significant difference between groups. However, bEVAR was associated with a significant postoperative increase in aortic TAWSS (median, 1.27 [IQR, 1.01-1.78] vs 3.17 [IQR, 2.69-4.91]; P = .005; preoperative vs postoperative), whereas fEVAR was associated with a significant reduction in aortic TAWSS postoperatively (median, 2.84 [IQR, 2.25-3.42] vs 1.91 [IQR, 1.34-2.48]; P = .005). The difference in relative change in aortic TAWSS between endograft strategies was also significant (+200.1% vs −31.3%; P = .001) (Fig 7, A). All 10 patients (100%) treated with fEVAR had postoperative decreases in TAWSS, whereas all 10 patients (100%) treated with bEVAR had postoperative increases in TAWSS. Representative patients with postoperative changes in paravisceral aortic TAWSS are demonstrated in Fig 7, B (fEVAR), and Fig 7, C (bEVAR).

Parameter analyses. The impact of prescribed flow rates, blood pressure, and vessel compliance parameters underwent a comprehensive independent systematic parameter analysis. Our investigation revealed that, despite variations in these parameters, branch perfusion (Supplementary Fig 2) and aortic as well as branch wall shear stress (Supplementary Fig 3) exhibited similar magnitude changes. Notably, higher in-flow rates and arterial pressure yielded only minimal increases in hemodynamic alterations, whereas lower in-flow and pressure parameters led to slight decreases in computed hemodynamic changes. It is worth noting that variations in pulse pressure did not seem to have a discernible influence on branch perfusion or TAWSS.

DISCUSSION

Endovascular aneurysm repair with multibranched and fenestrated endografts have been approved for commercial use in Europe for over a decade and in many centers have become the standard-of-care for treatment of complex aortic pathology.[2,6] In the United States, four-vessel fEVAR and bEVAR have demonstrated promising midterm outcomes in select centers with an investigational device exemption,[2,25] and aggressive adoption of this technology in the United States is likely if they were to become commercially available pending upcoming pivotal trials. We, thus, sought to elucidate potential differences in hemodynamic changes associated with the two predominate strategies for maintain renovisceral perfusion—fenestrated and branched grafts—using a patient-specific CFS pipeline validated for use in cardiovascular research.[26,27]

We conducted a multi-institutional, retrospective study comparing patients undergoing fEVAR and bEVAR for extent IV and higher thoracoabdominal aortic aneurysms. Although there were several distinct changes in hemodynamics associated with each strategy, we notably found that bEVAR was associated with a
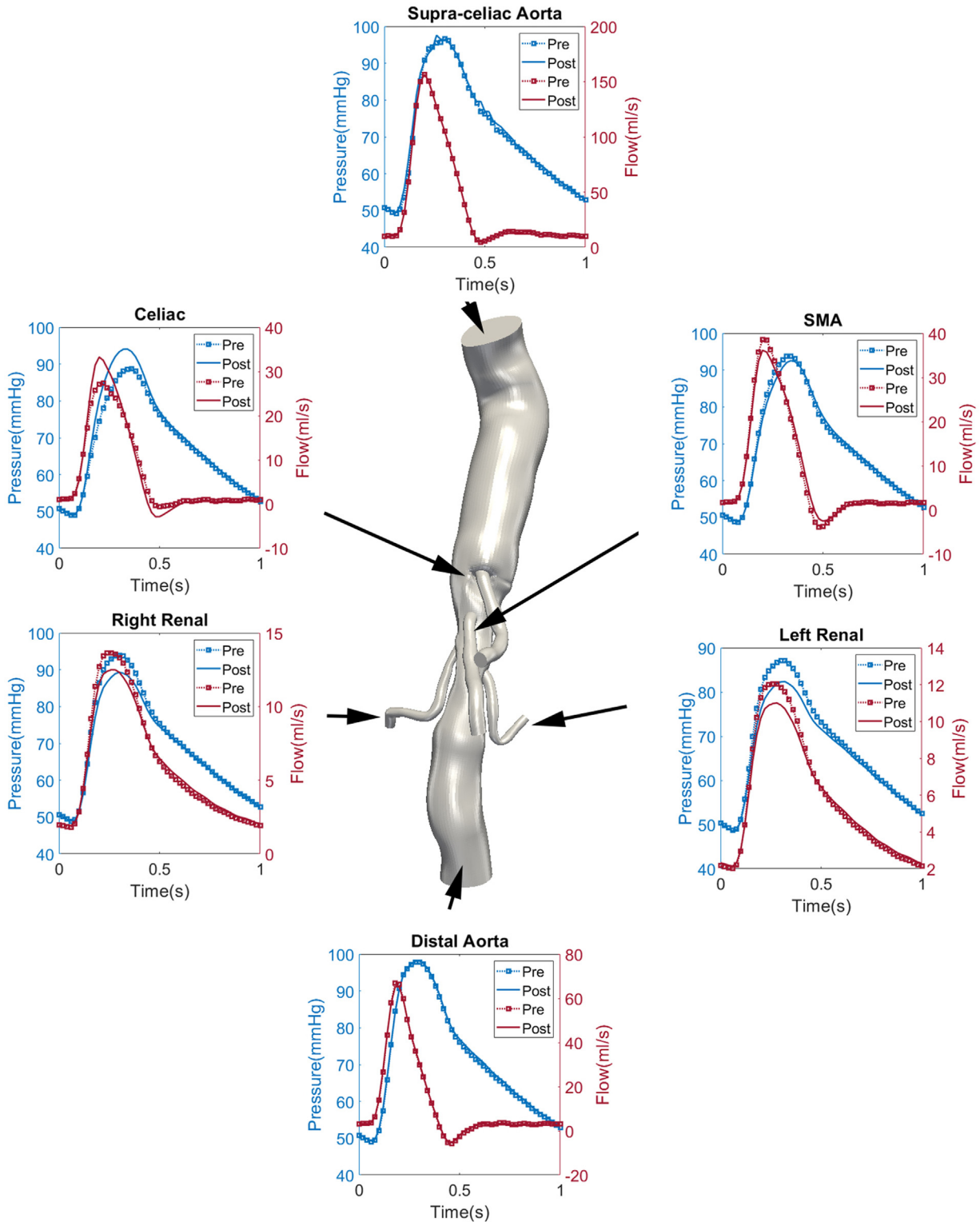
Fig 6. Representative flow simulation results for a single patient treated with four vessel branched endovascular aneurysm repair (bEVAR) resulting in minimal changes in celiac or superior mesenteric artery perfusion, but significant reduction in peak renal artery hemodynamics. Red lines represent flow waveforms; blue lines represent pressure waveforms. Dotted line represents preoperative state; solid line represents postoperative state. *SMA*, superior mesenteric artery.

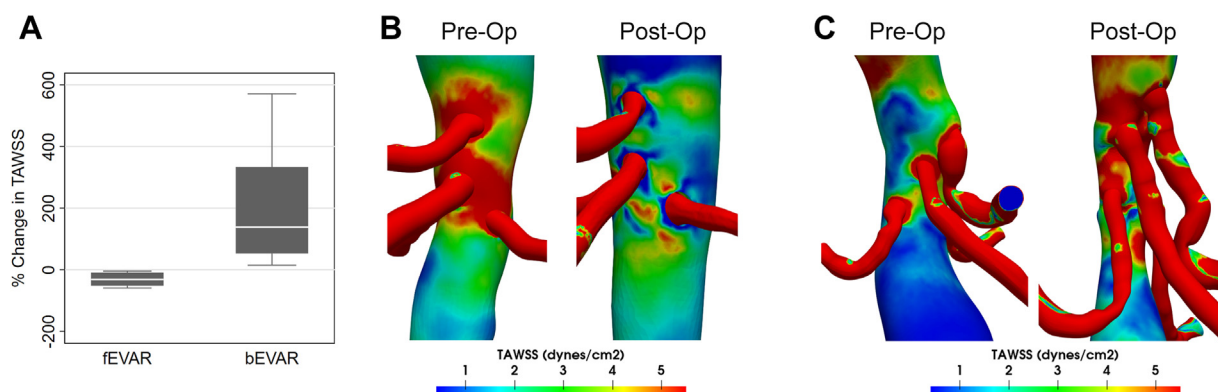**Fig 7. (A)** Relative changes in paravisceral aortic time-averaged wall shear stress (*TAWSS*) stratified by fenestrated endovascular aneurysm repair (fEVAR) and branched endovascular aneurysm repair (bEVAR) groups. **(B)** Three-dimensional contour plots demonstrating decreased paravisceral aortic wall shear stress postoperatively after fEVAR. Regions of subphysiological wall shear stress, shown in dark blue, predominate in regions adjacent to flared branch graft ostia. **(C)** Contour plot demonstrating increased paravisceral aortic wall shear stress post-operatively after bEVAR. Regions of supraphysiological wall shear stress, shown in red, predominate in the endograft proximal and adjacent to branch portals.

consistent decrease (~5%) in renal artery perfusion compared with preoperative values, whereas fEVAR was not associated with significant changes to renal perfusion. Importantly, there were no significant differences between celiac artery or SMA perfusion between the groups. TAWSS in the paravisceral aorta and branches varied significantly depending on endograft configuration, with bEVAR notably associated with large postoperative increases aortic TAWSS (~200%) compared with a moderate reduction in aortic TAWSS (~30%) associated with fEVAR. To our knowledge, these differences in computational estimated patient-specific hemodynamics between fEVAR and bEVAR have yet to be described.

It is important to discuss the clinical implications of these hemodynamic changes specifically with respect to the durability and patency of branch grafts. The long-term durability and patency of branch grafts remains a concerning issue in the endovascular management of complex aortic pathology. Mastracci et al[2] in a study of 650 patients treated with branched and fenestrated EVAR described a 16% estimated risk of branch-related reintervention over 5 years. Of these, renal branch occlusion or stenosis was the most frequent (11%), compared with risk of SMA events (4%) and celiac events (0.6%).[2] Interestingly, we found that renal branches after bEVAR were more often associated with decreased arterial pressure and flow rate compared with SMA or celiac artery branches, providing a possible hemodynamic explanation for higher rates of renal graft complications. This differential hemodynamic effect may be due to the longer length required for renal branches in addition to a U-shaped configuration required to conform with a cranially directed renal artery. In comparison, the SMA more often exhibits a caudally directed orientation, which is more conducive to antegrade branch

placement. In our study, renal branches with a U-shaped renal branch configuration often had large (>10%) decreases in peak perfusion metrics. In these arteries, we were able to visualize specific locations of hemodynamic abnormalities, such as mild lumen compression and flow recirculation. However, postoperative median TAWSS values in all renovisceral branches were well within homeostatic physiological values (10-70 dynes/cm^2)[24] after both fEVAR and bEVAR. Further CFD studies involving real-world cases of bEVAR branch occlusion are thus an important topic of future study to potentially correlate adverse branch hemodynamics to risk of patency loss.

Although branch hemodynamics were marginally affected after complex EVAR, we found significant postoperative changes in aortic TAWSS that were dichotomous between bEVAR and fEVAR. Physiologic wall shear stress in the nondiseased paravisceral abdominal aorta is normally in the range of 2.3 to 5.5 dynes/cm^2 under resting physiological conditions.[28,29] Preoperatively, bEVAR patients were found to have subphysiological median aortic wall sheer stress, which subsequently significantly increased to physiological levels postoperatively. This was likely due to the abrupt change in effective aortic diameter after endograft implantation owing to the smaller aortic lumen typically used in graft construction for bEVAR devices. In contrast, fEVAR patients were found to have physiological aortic TAWSS preoperatively; however, postoperatively was associated with a significant reduction in aortic TAWSS to subphysiological levels. This difference in aortic hemodynamics is important to consider, because a lower TAWSS is a well-known hemodynamic risk factor for thrombus formation owing to increasing local blood viscosity, erythrocyte aggregation, and platelet activation.[30-32] Wall shear stress-related indices have been shown to accurately identify regions of thrombus formation in untreated human abdominal

aortic aneurysms.[32-34] We found that low aortic TAWSS predominated in regions surrounding flared branch grafts and was consistent with areas of altered velocity streamlines and flow recirculation previously attributed to flared renal stent geometry.[14,21] Indeed, our group has previously studied thrombotic events after two-vessel fEVAR and found that reduced aortic TAWSS was associated with a higher risk of significant intra-luminal aortic thrombus development and renal stent occlusion.[35]

Studies using CFS in the setting of complex EVAR remain limited, in part owing to the large computational resources required to conduct patient-specific simulation.[14,15,17] Existing investigations have largely focused on computational bench testing using idealized, nonpatient-specific geometries. Kandail et al[14] studied the different endograft configurations for two-vessel fEVAR for renal arteries. They found that antegrade branches outperformed retrograde branches, but that both branch designs were inferior to fenestrated graft configurations in terms of maximizing renal flow rate. Similar to the present study, they found only small differences in renal flow rate (<1.5 mL/s) and did not vary substantial with varying aortic angulation or renal take-off angulation.[15] In another study, Suess et al[17] focused on evaluation of near wall hemodynamic parameters such as wall shear stress, relative residence time, and oscillatory shear index. They compared theoretical models of fenestrated, antegrade/retrograde branches, and a novel manifold graft design that uses a series of bifurcating antegrade branch stents deployed proximally in the thoracic aorta. Their study found qualitative differences in wall shear stress and shear indices between branch configurations, with the manifold design having more favorable near-wall hemodynamics compared with other designs. This result was attributed to the manifold graft using longer branch lengths with larger radius curvature, thus decreasing areas of flow separation and mixing. In our study, we found that all four visceral branches maintained normal physiological TAWSS parameters before and after bEVAR. However, the fenestrated configuration seemed to provide more stable hemodynamics in the renal arteries compared with branched configurations. Additional studies using both computational and bench-constructed in situ endograft models are required to further study these differences.

There are several limitations to this study that are worth discussion. First, our flow simulation results lack clinical validation. Computational estimated hemodynamics could be validated using either phase-contrast magnetic resonance imaging or duplex ultrasound examination to derive inlet and outlet branch waveforms. However, phase-contrast magnetic resonance imaging is expensive and not routinely clinically performed and duplex ultrasound examination-derived arterial waveforms suffer from significant user variability and are not part of routine surveillance protocols. Additional parameters such as arterial pressure would require invasive catheter-based studies, whereas other parameters such as TAWSS cannot be obtained using current clinical imaging modalities. Second, this study involved 10 representative patients in each cohort, which were selected retrospectively and thus prone to selection bias. Although a 20-patient cohort is relatively large in comparison with existing patient-based CFS studies, the low overall sample size limits statistical analyses and increases the possibility of a type II error. Furthermore, patients within the bEVAR group also were treated for a higher aneurysm extent. The increased length of aortic graft coverage could potentially result in differences between measured aortic inlet and outlet hemodynamics owing to differences in flow lumen. However, we attempted to minimize this difference by matching overall graft diameters between groups.

Another constraint in our study pertains to the absence of a clear distinction between the native vessel wall and the graft wall when calculating TAWSS. We did not explicitly specify which sections of the surface represented the graft and which were comprised of native tissue when comparing preoperative and postoperative data. This has an impact on the biological implications of our findings since TAWSS is well-documented to influence atherogenesis and endothelial function in the native intima, while its effect on prosthetic surfaces is not as well-understood. A more comprehensive examination of WSS results is also required to strengthen our assertions, and calculating the residence time for each branch may yield further valuable insights into the hemodynamic effects for future research. Finally, our simulations assume rigid, nondeformable walls. Although endografts behave as nearly rigid in vivo, native vessels are best modelled using deformable wall simulations by using coupled momentum methods to determine fluid-solid interaction. However, this often requires an order of magnitude increase in computational resources.[36] Other studies have also shown minimal differences between rigid vs deformable wall simulations on calculated hemodynamic parameters in the abdominal aorta.[37] Results from our study may also differ depending on overall graft designs using different manufacturers with varying graft geometry with respect to diameters and lengths of tapered segments or fenestration/branch portal diameters.

Strengths of our study include the use of patient-specific analysis using aortic geometries in a comparably larger cohort of real-world patients in relation to the existing literature. This adds significant clinical value because patient-derived models are inclusive of the nuances of native aortic morphology (eg irregular lumen boundaries, aortic angulation). Simulations were also performed using both preoperative and postoperative anatomy, enabling comparison of hemodynamic changes on a per-patient basis. As boundary conditions are held constant between operative states, this allowed for a highly sensitive method

of evaluating geometry-dependent changes in hemodynamics. To our knowledge, this study is the first to use these methods to compare patient-specific changes between fEVAR and bEVAR strategies. With improved accessibility to large-scale computational resources, CFS is a promising tool that may aid in future device design and endovascular planning in the modern era of complex endovascular aortic repair.

CONCLUSIONS

Patient-specific CFS is an emerging tool for evaluating the unique hemodynamic effects of complex EVAR. bEVAR may be associated with subtle decreases in renal perfusion and a large increase in aortic wall shear stress compared with fEVAR. Future studies are required to clinically validate these findings and correlate changes in simulated hemodynamics to adverse branch-related events.

AUTHOR CONTRIBUTIONS

Conception and design: KT, CD, SD, JL
Analysis and interpretation: KT, CD, WY, AM
Data collection: KT, CD, SD, AK
Writing the article: KT, CD
Critical revision of the article: KT, CD, SD, AK, WY, AM, JL
Final approval of the article: KT, CD, SD, AK, WY, AM, JL
Statistical analysis: KT, CD
Obtained funding: Not applicable
Overall responsibility: KT

DISCLOSURES

None.

REFERENCES

1. Suckow BD, Goodney PP, Columbo JA, et al. National trends in open surgical, endovascular, and branched-fenestrated endovascular aortic aneurysm repair in Medicare patients. *J Vasc Surg.* 2018;67:1690–1697.e1.
2. Mastracci TM, Greenberg RK, Eagleton MJ, Hernandez AV. Durability of branches in branched and fenestrated endografts. *J Vasc Surg.* 2013;57:926–933 [discussion: 933].
3. Simons JP, Shue B, Flahive JM, et al. Trends in use of the only Food and Drug Administration-approved commercially available fenestrated endovascular aneurysm repair device in the United States. *J Vasc Surg.* 2017;65:1260–1269.
4. Canavati R, Millen A, Brennan J, et al. Comparison of fenestrated endovascular and open repair of abdominal aortic aneurysms not suitable for standard endovascular repair. *J Vasc Surg.* 2013;57:362–367.
5. de Souza LR, Oderich GS, Farber MA, et al. Editor's choice — comparison of renal outcomes in patients treated by Zenith® fenestrated and Zenith® abdominal aortic aneurysm stent grafts in US prospective pivotal trials. *Eur J Vasc Endovasc Surg.* 2017;53:648–655.
6. Youssef M, Deglise S, Szopinski P, et al. A multicenter experience with a new fenestrated-branched device for endovascular repair of thoracoabdominal aortic aneurysms. *J Endovasc Ther.* 2018;25:209–219.
7. Raux M, Patel VI, Cochennec F, et al. A propensity-matched comparison of outcomes for fenestrated endovascular aneurysm repair and open surgical repair of complex abdominal aortic aneurysms. *J Vasc Surg.* 2014;60:858–863 [discussion: 863-864].
8. Jones AD, Waduud MA, Walker P, Stocken D, Bailey MA, Scott DJA. Meta-analysis of fenestrated endovascular aneurysm repair versus open surgical repair of juxtarenal abdominal aortic aneurysms over the last 10 years. *BJS open.* 2019;3:572–584.
9. Dossabhoy SS, Simons JP, Diamond KR, et al. Reinterventions after fenestrated or branched endovascular aortic aneurysm repair. *J Vasc Surg.* 2018;68:669–681.
10. Walker J, Kaushik S, Hoffman M, et al. Long-term durability of multibranched endovascular repair of thoracoabdominal and pararenal aortic aneurysms. *J Vasc Surg.* 2019;69:341–347.
11. Malkawi AH, Resch TA, Bown MJ, et al. Sizing fenestrated aortic stent-grafts. *Eur J Vasc Endovasc Surg.* 2011;41:311–316.
12. Banno H, Cochennec F, Marzelle J, Becquemin JP. Comparison of fenestrated endovascular aneurysm repair and chimney graft techniques for pararenal aortic aneurysm. *J Vasc Surg.* 2014;60:31–39.
13. Tricarico R, He Y, Laquian L, et al. Hemodynamic and anatomic predictors of renovisceral stent-graft occlusion following chimney endovascular repair of juxtarenal aortic aneurysms. *J Endovasc Ther.* 2017;24:880–888.
14. Kandail H, Hamady M, Xu XY. Effect of a flared renal stent on the performance of fenestrated stent-grafts at rest and exercise conditions. *J Endovasc Ther.* 2016;23:809–820.
15. Kandail H, Hamady M, Xu XY. Comparison of blood flow in branched and fenestrated stent-grafts for endovascular repair of abdominal aortic aneurysms. *J Endovasc Ther.* 2015;22:578–590.
16. Segalova PA, Venkateswara Rao KT, Zarins CK, Taylor CA. Computational modeling of shear-based hemolysis caused by renal obstruction. *J Biomech Eng.* 2012;134:1–7.
17. Suess T, Anderson J, Danielson L, et al. Examination of near-wall hemodynamic parameters in the renal bridging stent of various stent graft configurations for repairing visceral branched aortic aneurysms. *J Vasc Surg.* 2016;64:788–796.
18. Van Bakel TM, Arthurs CJ, Van Herwaarden JA, et al. A computational analysis of different endograft designs for Zone 0 aortic arch repair. *Eur J Cardiothorac Surg.* 2018;54:389–396.
19. Marzelle J, Presles E, Becquemin JP. Results and factors affecting early outcome of fenestrated and/or branched stent grafts for aortic aneurysms: a multicenter prospective study. *Ann Surg.* 2015;261:197–206.
20. Les AS, Yeung JJ, Schultz GM, Herfkens RJ, Dalman RL, Taylor CA. Supraceliac and infrarenal aortic flow in patients with abdominal aortic aneurysms: mean flows, waveforms, and allometric scaling relationships. *Cardiovasc Eng Technol.* 2010;1:39–51.
21. Tran K, Yang W, Marsden A, Lee JT. Patient-specific computational flow modelling for assessing hemodynamic changes following fenestrated endovascular aneurysm repair. *J Vasc Surg.* 2020;72:e182–e183.
22. Westerhof N, Lankhaar J-W, Westerhof BE. The arterial Windkessel. *Med Biol Eng Comput.* 2009;47:131–141.
23. Williams LR, Leggett RW. Reference values for resting blood flow to organs of man. *Clin Phys Physiol Meas.* 1989;10:187–217.
24. Malek AM, Alper SL, Izumo S. Hemodynamic shear stress and its role in atherosclerosis. *J Am Med Assoc.* 1999;282:2035–2042.
25. Oderich GS, Ribeiro M, Reis De Souza L, Hofer J, Wigham J, Cha S. Endovascular repair of thoracoabdominal aortic aneurysms using fenestrated and branched endografts. *J Thorac Cardiovasc Surg.* 2017;153:S32–S41.e7.
26. Updegrove A, Wilson NM, Merkow J, Lan H, Marsden AL, Shadden SC. SimVascular: an open source pipeline for cardiovascular simulation. *Ann Biomed Eng.* 2017;45:525–541.
27. Lan H, Updegrove A, Wilson NM, Maher GD, Shadden SC, Marsden AL. A re-engineered software interface and workflow for the open-source SimVascular cardiovascular modeling package. *J Biomech Eng.* 2018;140:0245011–02450111.
28. Cheng CP, Parker D, Taylor CA. Quantification of wall shear stress in large blood vessels using Lagrangian interpolation functions with cine phase-contrast magnetic resonance imaging. *Ann Biomed Eng.* 2002;30:1020–1032.
29. Les AS, Shadden SC, Figueroa CA, et al. Quantification of hemodynamics in abdominal aortic aneurysms during rest and exercise using magnetic resonance imaging and computational fluid dynamics. *Ann Biomed Eng.* 2010;38:1288–1313.
30. Snabre P, Bitbol M, Mills P. Cell disaggregation behavior in shear flow. *Biophys J.* 1987;51:795–807.
31. Nesbitt WS, Westein E, Tovar-Lopez FJ, et al. A shear gradient-dependent platelet aggregation mechanism drives thrombus formation. *Nat Med.* 2009;15:665–673.

32. Bluestein D, Niu L, Schoephoerster RT, Dewanjee MK. Steady flow in an aneurysm model: correlation between fluid dynamics and blood platelet deposition. *J Biomech Eng.* 1996;118:280—286.

33. Zambrano BA, Gharahi H, Lim C, et al. Association of intraluminal thrombus, hemodynamic forces, and abdominal aortic aneurysm expansion using longitudinal CT images. *Ann Biomed Eng.* 2016;44: 1502—1514.

34. Boyd AJ, Kuhn DCS, Lozowy RJ, Kulbisky GP. Low wall shear stress predominates at sites of abdominal aortic aneurysm rupture. *J Vasc Surg.* 2016;63:1613—1619.

35. Tran K, Feliciano K, Yang W, Marsden A, Dalman R, Lee J. Patient-specific changes in aortic hemodynamics are associated with thrombotic risk after fenestrated endovascular aneurysm repair with large diameter endografts. *JVS Vasc Sci.* 2021;3:219—231.

36. Figueroa CA, Vignon-Clementel IE, Jansen KE, Hughes TJR, Taylor CA. A coupled momentum method for modeling blood flow in three-dimensional deformable arteries. *Comput Methods Appl Mech Eng.* 2006;195:5685—5706.

37. Looyenga EM, Gent SP. Examination of fluid-structure interaction in stent grafts and its hemodynamic implications. *Front Biomed Dev 2018.* 2018:12—16.